Decoupled Multi-Port Impedance Modelling Method of Transmission Network in Inverter-Fed Power Plant

Zhou, Weihua; Wang, Yanbo; Chen, Zhe

Published in:
Proceedings of the 6th international conference on smart grid

DOI (link to publication from Publisher):
10.1109/ISGWCP.2018.8634563

Publication date:
2018

Document Version
Accepted author manuscript, peer reviewed version

Decoupled Multi-Port Impedance Modelling Method of Transmission Network in Inverter-Fed Power Plant

Weihua Zhou*, Yanbo Wang†, and Zhe Chen‡
Department of Energy Technology
Aalborg University
Aalborg, Denmark
*wez@et.aau.dk, †ywa@et.aau.dk, ‡zch@et.aau.dk

***Abstract*—This paper presents a decoupled multi-port impedance modelling method of transmission network for stability analysis of inverter-fed power plant. The decoupled three-port and four-port impedance model are first derived. On the basis of them, multi-port impedance model of transmission network are deduced, where multiple branches-based transmission network is modelled by means of Norton equivalent circuit. In addition, stability analysis based on proposed impedance network modelling method is performed. Simulation results are given to validate effectiveness of the proposed decoupled multi-port impedance modelling and stability analysis method. The proposed modelling method is able to simplify impedance modelling procedure, which performs impedance based stability analysis for inverter-fed power plant with complicated transmission network in a computation-less way.**

***Index Terms*—Decoupled impedance modelling, inverter-fed power plant, impedance-based stability analysis, transmission network.**

I. Introduction

The increasing penetration of renewable energies, such as wind energy and solar energy, are promoting the application of distributed power generation. Solid state interface-based power converters are intensively adopted to integrate renewable energies into power systems [1]. To enhance power quality, passive components such as LCL and L filters are commonly used to mitigate high-order harmonics. However, the interaction between inner control loops and passive components can cause system resonance as variation of grid impedance in a wide frequency range [2]–[6]. Therefore, it is significant to develop modelling and analysis method for revealing mechanism and identifying possibility of oscillation phenomena at early planning stage of power plant.

Stability issues of multiple grid-connected inverter (GCI) system have been widely addressed in [4], [7]–[17]. Impedance-based stability criterion (IBSC) has been originally adopted to predict the stability issue of single GCI-based power plant [18]. The main disadvantage of IBSC is that only local stability can be predicted at a specific point [10]. To identify global stability, IBSC should be performed multiple times at all buses, if right-half-plane (RHP) poles of impedance ratios of load and source parts is not calculated [13], [16], [17]. However, it is not easy to implement stability assessment in a large-scale power system with complicated transmission network. Most of existing works always simplify or ignore transmission lines (TLs)/power cables impedance. For example, only the TL impedance between point of common connection (PCC) and grid is considered in [7]–[10], [12], [15]. The TLs impedance between the GCIs are considered in [13], [14], [17]. In addition, the TLs impedance between the GCIs and buses are considered in [11], [16]. Few papers simultaneously take the three kinds of TLs impedance into account. In [19], [20], the impedance matrix models of all components are first established in unified dq frame. Then, the unified dq-frame impedance network model is established by merging all individual impedance matrix models. However, the computation of system impedance matrix tends to cause high computational burdens, which weakens stability analysis efficiency. In [11], [21], a long transmission cable is modelled as a decoupled two-port network, where terminal impedance of long transmission cable is represented as the impedance of controlled voltage/current sources. The network modelling method is able to simplify IBSC. However, the modelling method fails to be implemented in a large-scale power system with complicated transmission network.

To perform stability assessment in inverter-fed power plant with complicated transmission network, this paper presents a decoupled multi-port impedance model of transmission network to assess stability issue of GCIs system. Main contributions in this paper are explained as follows. (1) Effect of TLs impedance on system stability is considered. (2) A decoupled multi-port impedance modelling method is established, which is able to simplify IBSC in inverter-fed power plant with complicated transmission network. Also, the modelling method can be flexibly applied in various network structures.

This work was supported by the ForskEL and EUDP Project "Voltage Control and Protection for a Grid towards 100% Power Electronics and Cable Network (COPE)" (Project No.: 880063).

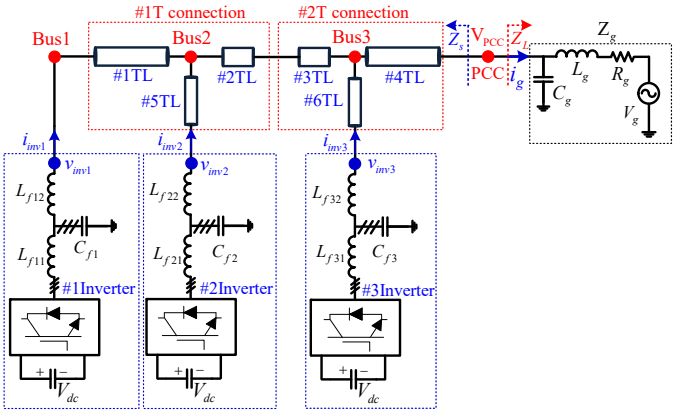

Fig. 1. Studied power plant diagram consisting of three GCIs and TLs.

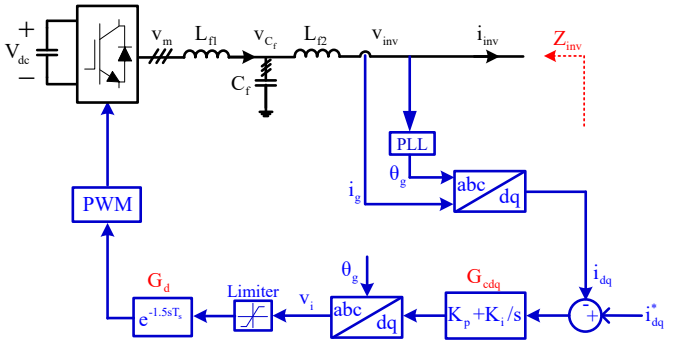

Fig. 2. Grid current control loop of GCI.

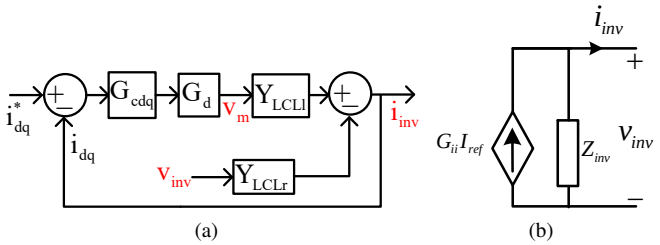

Fig. 3. Equivalent model of GCI. (a) Block diagram of grid current control loop; (b) Norton equivalent circuit model of GCI.

II. System Description

Fig. 1 shows circuit configuration of studied inverter-fed power plant, which consists of three GCIs and TLs. There are two main existing IBSCs performing stability analysis of the power plant. The first one is to perform stability analysis by adding system components (GCI and TL) from left to right step by step in a sequential way, where IBSC should be implemented at bus 1, 2, 3 and PCC without calculating the right half plane (RHP) poles of the impedance ratios of load and source parts. The second one is to perform IBSC one time at a specific point with calculating the RHP poles of the impedance ratio [17]. The first approach is more competitive for multiple GCIs-based power plant, since the order of the impedance ratio can be very high, which leads to RHP poles calculation of the impedance ratio time-consuming.

However, the first approach needs to calculate four impedance formulas, which are the left parts of bus 1, bus 2, bus 3 and PCC, respectively. The repetitive process makes the IBSC tedious. In principle, the GCIs can be modelled as Norton equivalent circuits [18]. One assumption is that if the transmission networks shown as #1T connection and #2T connection in Fig. 1 can also be represented as Norton/Thevenin equivalent circuits, the analysis process may be simplified, which will be explained in next section.

III. Proposed Impedance Modelling Method

In this section, impedance models of GCI and transmission network are first established. Then, system impedance model of the exemplified power plant as shown in Fig. 1 is established. The stability analysis method based on the established system impedance model is finally explained.

A. Impedance modelling of GCI

Fig. 2 shows the control diagram of LCL-filtered GCI with grid current feedback. Current controller is used to enable the GCI. Time delay of digital control system (G_d) is considered, which consists of computation delay (T_s) and PWM delay ($0.5T_s$).

Fig. 3(a) shows equivalent model of GCI, where PLL and coordinate transformation are not considered, since the PLL only influences the inverter output impedance in low-frequency range.

The inverter output impedance can be derived as (1) [6].

$$Z_{inv} = -\frac{v_{inv}}{i_{inv}} = \frac{1 + G_{cdq}G_dY_{LCLl}}{Y_{LCLr}} \tag{1}$$

where

$$Y_{LCLl} = \left.\frac{i_{inv}}{v_m}\right|_{v_{inv}=0} = \frac{Z_{Cf}}{(Z_{Cf}//sL_{f2} + sL_{f1})(Z_{Cf} + sL_{f2})}$$
$$Y_{LCLr} = \left.\frac{i_{inv}}{v_{inv}}\right|_{v_m=0} = \frac{1}{(Z_{Cf}//sL_{f1} + sL_{f2})} \tag{2}$$

where $Z_{Cf} = \frac{1}{sC_f}$.

Norton equivalent circuit can be established, shown as in Fig. 3(b), which will be integrated into system impedance model.

B. Impedance modelling of transmission network

The decoupled three-port impedance model of three branches-based transmission network is first established, followed by extension to multiple branches-based transmission network.

1) Three-port impedance model of T-connected transmission network: Fig. 4 shows a T-connected transmission network, where the impedances of the three branches are Z_1, Z_2, Z_3 (TL 4 is not considered here). Assuming three terminal voltages are v_1, v_2 and v_3, respectively. Kirchhoff's current law (KCL) can be applied at node v, shown as in (3).

$$i_1 + i_2 + i_3 = \frac{v - v_1}{Z_1} + \frac{v - v_2}{Z_2} + \frac{v - v_3}{Z_3} = 0 \tag{3}$$

The node voltage v can be obtained as (4).

$$v = f(v_1, v_2, v_3) = \frac{Z_1Z_2v_3 + Z_2Z_3v_1 + Z_1Z_3v_2}{Z_1Z_2 + Z_2Z_3 + Z_1Z_3} \tag{4}$$

Then, three currents i_1, i_2 and i_3 can be obtained by Ohm's law as (5).

$$\begin{aligned} i_1 &= \frac{v - v_1}{Z_1} = \frac{Z_2v_3 + Z_3v_2 - (Z_2 + Z_3)v_1}{Z_1Z_2 + Z_2Z_3 + Z_1Z_3} \\ i_2 &= \frac{v - v_2}{Z_2} = \frac{Z_1v_3 + Z_3v_1 - (Z_1 + Z_3)v_2}{Z_1Z_2 + Z_2Z_3 + Z_1Z_3} \\ i_3 &= \frac{v - v_3}{Z_3} = \frac{Z_1v_2 + Z_2v_1 - (Z_1 + Z_2)v_3}{Z_1Z_2 + Z_2Z_3 + Z_1Z_3} \end{aligned} \tag{5}$$

(5) can be represented as (6).

$$\begin{aligned} i_1 &= f_1(v_1, v_2, v_3) = -\frac{v_1}{Z_{1sh}} + i_1' \\ i_2 &= f_2(v_1, v_2, v_3) = -\frac{v_2}{Z_{2sh}} + i_2' \\ i_3 &= f_3(v_1, v_2, v_3) = -\frac{v_3}{Z_{3sh}} + i_3' \end{aligned} \tag{6}$$

where

$$\begin{aligned} i_1' &= \frac{Z_2v_3 + Z_3v_2}{Z_1Z_2 + Z_2Z_3 + Z_1Z_3} \\ i_2' &= \frac{Z_1v_3 + Z_3v_1}{Z_1Z_2 + Z_2Z_3 + Z_1Z_3} \\ i_3' &= \frac{Z_1v_2 + Z_2v_1}{Z_1Z_2 + Z_2Z_3 + Z_1Z_3} \end{aligned} \tag{7}$$

$$\begin{aligned} Z_{1sh} &= \frac{Z_1Z_2 + Z_2Z_3 + Z_1Z_3}{Z_2 + Z_3} \\ Z_{2sh} &= \frac{Z_1Z_2 + Z_2Z_3 + Z_1Z_3}{Z_1 + Z_3} \\ Z_{3sh} &= \frac{Z_1Z_2 + Z_2Z_3 + Z_1Z_3}{Z_1 + Z_2} \end{aligned} \tag{8}$$

According to (6), the three-port impedance model of Fig. 4 can be established, as shown in Fig. 5. In addition, the three impedances of the Norton equivalent circuits Z_{1sh}, Z_{2sh} and Z_{3sh} in Fig. 5 are the three terminal impedances with the other two terminals short-circuited Z_{out1}, Z_{out2} and Z_{out3}, derived as (9).

$$\begin{aligned} Z_{1sh} &= \left.\frac{-v_1}{\frac{-v_1}{Z_{1sh}} + i_1'}\right|_{i_1'=0} = \left.\frac{-v_1}{i_1}\right|_{v_2=v_3=0} = Z_{out1} \\ Z_{2sh} &= \left.\frac{-v_2}{\frac{-v_2}{Z_{2sh}} + i_2'}\right|_{i_2'=0} = \left.\frac{-v_2}{i_2}\right|_{v_1=v_3=0} = Z_{out2} \\ Z_{3sh} &= \left.\frac{-v_3}{\frac{-v_3}{Z_{3sh}} + i_3'}\right|_{i_3'=0} = \left.\frac{-v_3}{i_3}\right|_{v_1=v_2=0} = Z_{out3} \end{aligned} \tag{9}$$

It can be seen that the established three-port impedance model of the T-connected transmission network makes the terminal impedance with the other two terminals short-circuited apparent and visible.

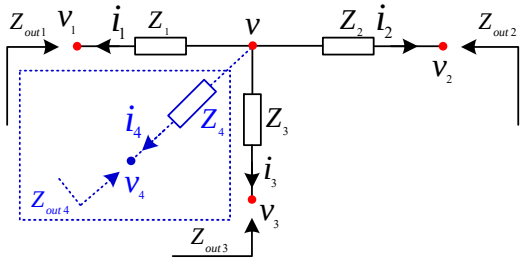

Fig. 4. Multi-port transmission network.

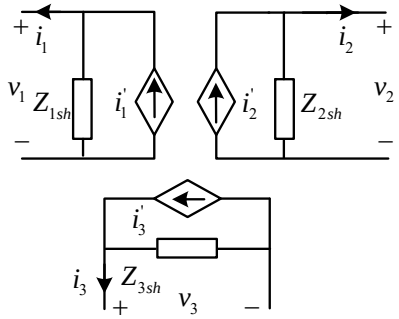

Fig. 5. Three-port impedance model of T-connected transmission network as shown in Fig. 4.

2) Multi-port impedance model modelling: Based on the derivation process of decoupled three-port impedance model of T-connected transmission network, a decoupled four-port impedance model of the transmission network in Fig. 4 (TL 4 is considered here) can be established. Equivalent decoupled four-port impedance model is shown in Fig. 6. The impedance representations are shown as (10).

$$\begin{aligned} Z_{1sh}^* &= \frac{Z_2Z_3Z_4 + Z_1Z_3Z_4 + Z_1Z_2Z_4 + Z_1Z_2Z_3}{Z_3Z_4 + Z_2Z_4 + Z_2Z_3} \\ Z_{2sh}^* &= \frac{Z_2Z_3Z_4 + Z_1Z_3Z_4 + Z_1Z_2Z_4 + Z_1Z_2Z_3}{Z_3Z_4 + Z_1Z_4 + Z_1Z_3} \\ Z_{3sh}^* &= \frac{Z_2Z_3Z_4 + Z_1Z_3Z_4 + Z_1Z_2Z_4 + Z_1Z_2Z_3}{Z_2Z_4 + Z_1Z_4 + Z_1Z_2} \\ Z_{4sh}^* &= \frac{Z_2Z_3Z_4 + Z_1Z_3Z_4 + Z_1Z_2Z_4 + Z_1Z_2Z_3}{Z_2Z_3 + Z_1Z_3 + Z_1Z_2} \end{aligned} \tag{10}$$

Comparing (8) with (10), the impedance representations of the decoupled m-port impedance model of the m branches-based transmission network can be derived as (11).

$$Z_{ksh} = \frac{\sum_{i=1}^{m}\left(\prod_{j=1,j\neq i}^{m} Z_j\right)}{\sum_{i=1,i\neq k}^{m}\left(\prod_{j=1,j\neq i,j\neq k}^{m} Z_j\right)} \quad k = 1, 2...m \tag{11}$$

It indicates that the proposed impedance modelling method for transmission network is not limited to the T-connected case in Fig. 1. However, for simplicity, only the T-connected case is studied in this paper.

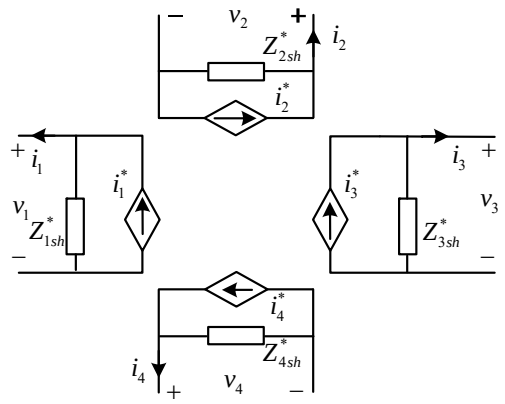

Fig. 6. Four-port impedance model of four branches-based transmission network as shown in Fig. 4.

C. Stability analysis based on proposed impedance network modelling method

The proposed impedance model of the studied power plant in Fig. 1 can be established by combining Fig. 3 and Fig. 5, as shown in Fig. 7. The impedance formulas in this model are in interest for stability analysis. Therefore, the formulas are listed as (12) and (13), which are in a similar form of (8).

$$\begin{aligned} Z_{11sh} &= \frac{Z_{TL1}Z_{TL2}+Z_{TL1}Z_{TL5}+Z_{TL2}Z_{TL5}}{Z_{TL2}+Z_{TL5}} \\ Z_{12sh} &= \frac{Z_{TL1}Z_{TL2}+Z_{TL1}Z_{TL5}+Z_{TL2}Z_{TL5}}{Z_{TL1}+Z_{TL5}} \\ Z_{13sh} &= \frac{Z_{TL1}Z_{TL2}+Z_{TL1}Z_{TL5}+Z_{TL2}Z_{TL5}}{Z_{TL1}+Z_{TL2}} \end{aligned} \tag{12}$$

$$\begin{aligned} Z_{21sh} &= \frac{Z_{TL3}Z_{TL4}+Z_{TL4}Z_{TL6}+Z_{TL3}Z_{TL6}}{Z_{TL4}+Z_{TL6}} \\ Z_{22sh} &= \frac{Z_{TL3}Z_{TL4}+Z_{TL4}Z_{TL6}+Z_{TL3}Z_{TL6}}{Z_{TL3}+Z_{TL6}} \\ Z_{23sh} &= \frac{Z_{TL3}Z_{TL4}+Z_{TL4}Z_{TL6}+Z_{TL3}Z_{TL6}}{Z_{TL3}+Z_{TL4}} \end{aligned} \tag{13}$$

When performing IBSC2 and IBSC3, the impedance ratio of the right part and left part should be calculated to check whether the Nyquist stability criterion is met or not. Therefore, Z_{12sh} and Z_{22sh} should be modified to include the terminal impedances of #1Inverter, #2Inverter and #3Inverter, shown as in (14) and (15).

After obtaining the necessary impedance formulas in Fig. 7, the stability issue of the radial power plant can be assessed by applying the IBSC three times. In detail, IBSC1, IBSC2 and IBSC3 check the impedance ratios Z_{11sh}/Z_{inv1}, Z_{21sh}/Z'_{12sh} and Z_g/Z'_{22sh}, respectively.

In principle, the proposed impedance modelling method is applicable for power plant with more GCIs. The formulas of the decoupled three-port impedance network can be derived in a recursive way. For example, assuming there are n T-connected TL networks in the power plant, and the impedances of three branches #$(2n-1)$, #$(2n)$ and #$(3n)$ of the nth TL network are $Z_{TL(2n-1)}$, $Z_{TL(2n)}$ and $Z_{TL(3n)}$, respectively. The impedance formulas of the established nth decoupled three-port impedance network can be derived as in (16), and the modified formula of Z_{n2sh} is shown in (17).

The proposed impedance network modelling and stability analysis method is now used to analyze the stability issue of the studied radial power plant. Assuming the parameters of the three GCIs are the same, and Table I shows the parameters of single GCI and the parameters of the capacitive grid impedance.

TABLE I
PARAMETERS OF THE GCI AND GRID

Parameter	Value
dc-link voltage V_{dc}	800V
Grid fundamental frequency	50Hz
Inverter side filter inductor L_{f1}	5mH
Grid side filter inductor L_{f2}	5mH
Filter capacitor C_f	1μF
Grid capacitance C_g	8μF
Grid inductance L_g	1mH
Grid resistance R_g	0.1Ω
Switching frequency f_s	10kHz
Sampling frequency f_{samp}	10kHz
Grid voltage (phase-to-phase) V_g	380V
Proportional gain of current controller K_p	40
Integral gain of current controller K_i	2000
Proportional gain of PLL K_p	0.7
Integral gain of PLL K_i	3.2
Current reference value i_d^*	30A
Current reference value i_q^*	0

If $L_{LTC1}=L_{LTC5}=L_{LTC6}=5$mH, $L_{LTC2}=L_{LTC3}=L_{LTC4}=0.5$mH and $C_g=8\mu$F, $L_g=1$mH, $R_g=0.15\Omega$, three Nyquist plots of the impedance ratios Z_{11sh}/Z_{inv1}, Z_{21sh}/Z'_{12sh} and Z_g/Z'_{22sh} are drawn in Fig. 8. It can be seen that the last Nyquist plot encircles point (-1, j0) one time, indicating that the system is unstable. In addition, if grid resistance is increased from 0.15 Ω to 0.3Ω. The three Nyquist plots are drawn in Fig. 9 again. It can be seen that all of them do not encircle point (-1, j0), indicating that the system is stable.

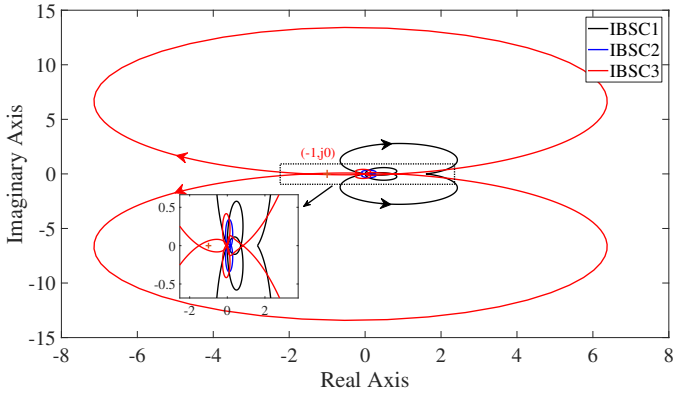

Fig. 8. Nyquist plots of three impedance ratios of three GCIs case with $C_g=8\mu$F, $L_g=1$mH, $R_g=0.15\Omega$ and $L_{LTC1}=L_{LTC5}=L_{LTC6}=5$mH, $L_{LTC2}=L_{LTC3}=L_{LTC4}=0.5$mH.

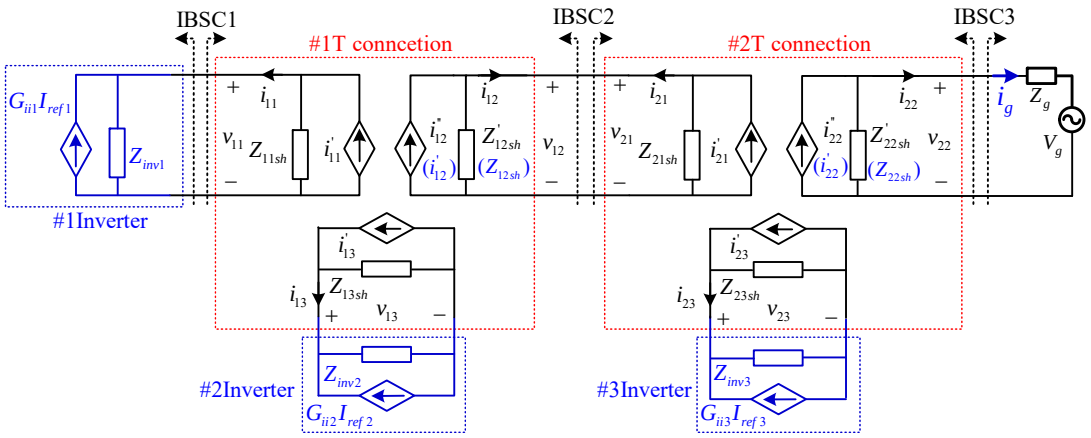

Fig. 7. Decoupled impedance network model of the power plant as shown in Fig. 1.

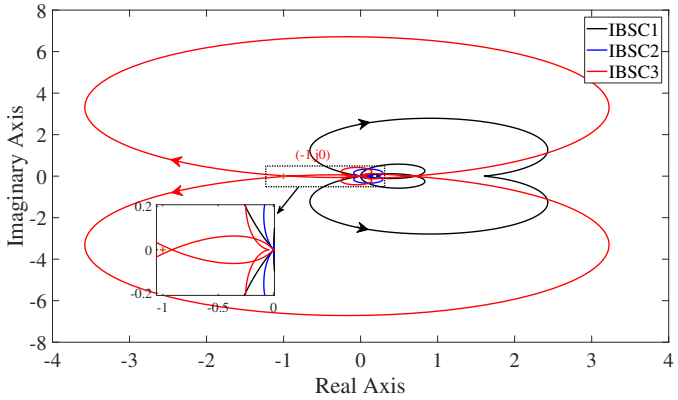

Fig. 9. Nyquist plots of three impedance ratios of three GCIs case with $C_g = 8\mu$F, $L_g = 1$mH, $R_g = 0.3\Omega$ and $L_{LTC1} = L_{LTC5} = L_{LTC6} = 5$mH, $L_{LTC2} = L_{LTC3} = L_{LTC4} = 0.5$mH.

IV. Simulation Verification

In this section, the fact that more GCIs and the three kinds of TLs can make system unstable is first revealed by time-domain simulation waveforms, indicating the necessity to take all of the three kinds of TLs impedance into account. Then, time-domain simulation results are given to validate effectiveness of the proposed impedance network modelling method.

A. The effect of GCIs number and the three kinds of TLs on system stability

#3 inverter and #2T connection as shown in Fig. 1 are not considered, and the studied power plant now consists of two GCIs. Fig. 10 shows the simulation result about grid current i_g, and it can be seen that the system is stable. As a comparison, Fig. 11 gives the simulation result about grid current i_g of three GCIs case under the same grid condition, and it can be seen that the system is unstable. The power plant may become unstable as increase of inverter number.

In addition, if inductance of #4TL between bus 3 and PCC increases from 4 mH to 7 mH, grid current i_g becomes stable again, as shown in Fig. 12. From Figs. 10, 11 and 12, it can

$$Z'_{12sh} = \frac{(Z_{TL1} + Z_{inv1})Z_{TL2} + (Z_{TL1} + Z_{inv1})(Z_{TL5} + Z_{inv2}) + Z_{TL2}(Z_{TL5} + Z_{inv2})}{(Z_{TL1} + Z_{inv1}) + (Z_{TL5} + Z_{inv2})} \tag{14}$$

$$Z'_{22sh} = \frac{(Z_{TL3} + Z'_{12sh})Z_{TL4} + (Z_{TL3} + Z'_{12sh})(Z_{TL6} + Z_{inv3}) + Z_{TL4}(Z_{TL6} + Z_{inv3})}{(Z_{TL3} + Z'_{12sh}) + (Z_{TL6} + Z_{inv3})} \tag{15}$$

$$\begin{aligned}
Z_{n1sh} &= \frac{Z_{TL(2n-1)}Z_{TL(2n)} + Z_{TL(2n-1)}Z_{TL(3n)} + Z_{TL(2n)}Z_{TL(3n)}}{Z_{TL(2n)} + Z_{TL(3n)}} \\
Z_{n2sh} &= \frac{Z_{TL(2n-1)}Z_{TL(2n)} + Z_{TL(2n-1)}Z_{TL(3n)} + Z_{TL(2n)}Z_{TL(3n)}}{Z_{TL(2n-1)} + Z_{TL(3n)}} \\
Z_{n3sh} &= \frac{Z_{TL(2n-1)}Z_{TL(2n)} + Z_{TL(2n-1)}Z_{TL(3n)} + Z_{TL(2n)}Z_{TL(3n)}}{Z_{TL(2n-1)} + Z_{TL(2n)}}
\end{aligned} \tag{16}$$

$$Z'_{n2sh} = \frac{(Z_{TL(2n-1)} + Z'_{(n-1)2sh})Z_{TL(2n)} + (Z_{TL(2n-1)} + Z'_{(n-1)2sh})(Z_{TL(3n)} + Z_{invn}) + Z_{TL(2n)}(Z_{TL(3n)} + Z_{invn})}{(Z_{TL(2n-1)} + Z'_{(n-1)2sh}) + (Z_{TL(3n)} + Z_{invn})} \tag{17}$$

be concluded that both the TL impedance and the number of GCIs can affect system stability.

B. Verification of the stability analysis method based on the proposed impedance network model

Fig. 13 shows the time-domain simulation result i_g under the same grid condition as Fig. 8. The simulation result agrees with the IBSC result in Fig. 8. It can be seen that the multi-step IBSC based on the established impedance network model predicts the instability phenomenon.

Similarly, Fig. 14 shows the time-domain simulation result i_g under the same grid condition as Fig. 9. The simulation result agrees with the IBSC result in Fig. 9. It can be seen that the multi-step IBSC based on the established impedance network model predicts the stability phenomenon.

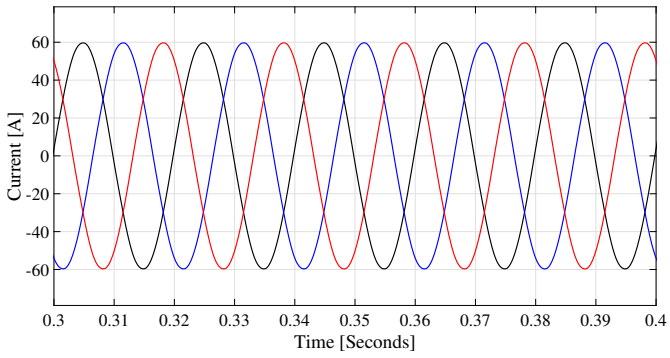

Fig. 10. Grid current i_g of two GCIs case with $C_g = 8\mu$F, $L_g = 1$mH, $R_g = 0.1\Omega$ and $L_{LTC1} = L_{LTC5} = 5$mH, $L_{LTC2} = 4$mH.

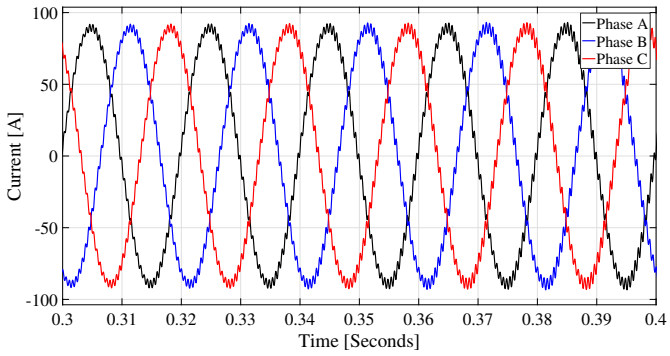

Fig. 11. Grid current i_g of three GCIs case with $C_g = 8\mu$F, $L_g = 1$mH, $R_g = 0.1\Omega$ and $L_{LTC1} = L_{LTC3} = L_{LTC5} = L_{LTC6} = 5$mH, $L_{LTC4} = 4$mH.

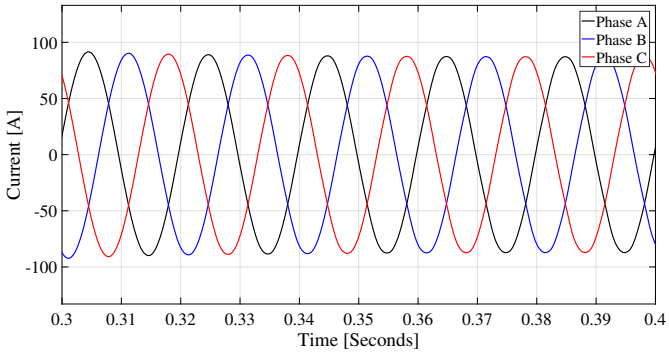

Fig. 12. Grid current i_g of three GCIs case with $C_g = 8\mu$F, $L_g = 1$mH, $R_g = 0.1\Omega$ and $L_{LTC1} = L_{LTC3} = L_{LTC5} = L_{LTC6} = 5$mH, $L_{LTC4} = 7$mH.

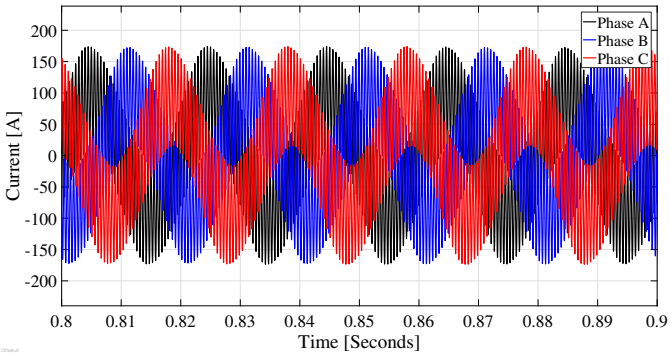

Fig. 13. Grid current i_g of three GCIs with $C_g = 8\mu$F, $L_g = 1$mH, $R_g = 0.15\Omega$ and $L_{LTC1} = L_{LTC5} = L_{LTC6} = 5$mH, $L_{LTC2} = L_{LTC3} = L_{LTC4} = 0.5$mH.

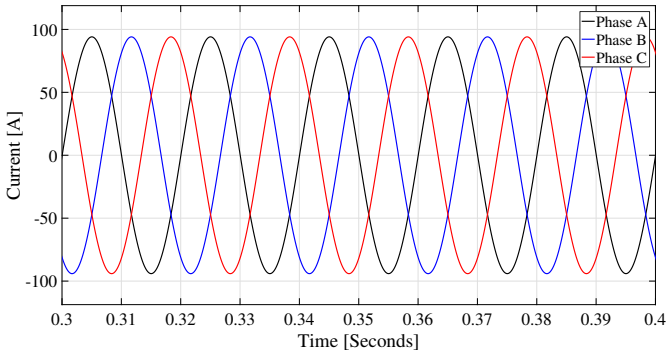

Fig. 14. Grid current of three GCIs with $C_g = 8\mu$F, $L_g = 1$mH, $R_g = 0.3\Omega$ and $L_{LTC1} = L_{LTC5} = L_{LTC6} = 5$mH, $L_{LTC2} = L_{LTC3} = L_{LTC4} = 0.5$mH.

V. Conclusions

This paper presents a decoupled multi-port impedance modelling method of transmission network for stability analysis of inverter-fed power plant. Multi-port impedance model of transmission network are modelled by means of Norton equivalent circuit. Also, stability analysis based on proposed impedance network modelling method is performed. Simulation results show that the proposed decoupled multi-port impedance modelling method is able to simplify modelling procedure of

transmission network, which can perform stability analysis for inverter-fed power plant with complicated transmission network. Also, the modelling method can be flexibly applied in various network structures.

REFERENCES

[1] F. Blaabjerg, Z. Chen, and S. B. Kjaer, "Power electronics as efficient interface in dispersed power generation systems," *IEEE Trans. Power Electron.*, vol. 19, no. 5, pp. 1184–1194, Sep. 2004.

[2] J. H. Enslin and P. J. Heskes, "Harmonic interaction between a large number of distributed power inverters and the distribution network," *IEEE Trans. Power Electron.*, vol. 19, no. 6, pp. 1586–1593, Nov. 2004.

[3] H. Wang, W. Mingli, and J. Sun, "Analysis of low-frequency oscillation in electric railways based on small-signal modeling of vehicle-grid system in dq frame," *IEEE Trans. Power Electron.*, vol. 30, no. 9, pp. 5318–5330, Sep. 2015.

[4] E. Ebrahimzadeh, F. Blaabjerg, X. Wang, and C. L. Bak, "Bus participation factor analysis for harmonic instability in power electronics based power systems," *IEEE Trans. Power Electron.*, vol. 33, no. 12, pp. 10 341–10 351, Dec. 2018.

[5] Y. Wang, X. Wang, F. Blaabjerg, and Z. Chen, "Harmonic resonance assessment of multiple paralleled grid-connected inverters system," in *Future Energy Electronics Conference and ECCE Asia (IFEEC-ECCE Asia)*. IEEE, 2017, pp. 2070–2075.

[6] W. Zhou, Y. Wang, and Z. Chen, "Reduced-order modelling method of grid-connected inverter with long transmission cable," in *Annual Conference of the IEEE Industrial Electronics Society (IECON)*. IEEE, 2018, pp. 1–8.

[7] J. L. Agorreta, M. Borrega, J. Lopez, and L. Marroyo, "Modeling and control of N-paralleled grid-connected inverters with LCL filter coupled due to grid impedance in PV plants," *IEEE Trans. Power Electron.*, vol. 26, no. 3, pp. 770–785, Mar. 2011.

[8] J. He, Y. W. Li, D. Bosnjak, and B. Harris, "Investigation and active damping of multiple resonances in a parallel-inverter-based microgrid," *IEEE Trans. Power Electron.*, vol. 28, no. 1, pp. 234–246, Jan. 2013.

[9] M. Lu, X. Wang, P. C. Loh, and F. Blaabjerg, "Resonance interaction of multiparallel grid-connected inverters with LCL filter," *IEEE Trans. Power Electron.*, vol. 32, no. 2, pp. 894–899, Feb. 2017.

[10] Y. Wang, X. Wang, F. Blaabjerg, and Z. Chen, "Frequency scanning-based stability analysis method for grid-connected inverter system," in *Future Energy Electronics Conference and ECCE Asia (ECCE Asia)*. IEEE, 2017, pp. 1575–1580.

[11] X. Zhang, H. S.-h. Chung, L. L. Cao, J. P. W. Chow, and W. Wu, "Impedance-based stability criterion for multiple offshore inverters connected in parallel with long cables," in *Energy Conversion Congress and Exposition (ECCE)*. IEEE, 2017, pp. 3383–3389.

[12] M. K. Bakhshizadeh, F. Blaabjerg, J. Hjerrild, L. Kocewiak, and C. L. Bak, "Improving the impedance based stability criterion by using the vector fitting method," *IEEE Trans. Energy Convers.*, Early Access.

[13] W. Cao, X. Zhang, Y. Ma, and F. Wang, "Stability criterion and controller parameter design of radial-line renewable systems with multiple inverters," in *Applied Power Electronics Conference and Exposition (APEC)*. IEEE, 2016, pp. 2229–2236.

[14] X. Wang, F. Blaabjerg, and P. C. Loh, "Proportional derivative based stabilizing control of paralleled grid converters with cables in renwable power plants," in *Energy Conversion Congress and Exposition (ECCE)*. IEEE, 2014, pp. 4917–4924.

[15] Q. Ye, R. Mo, Y. Shi, and H. Li, "A unified impedance-based stability criterion (UIBSC) for paralleled grid-tied inverters using global minor loop gain (GMLG)," in *Energy Conversion Congress and Exposition (ECCE)*. IEEE, 2015, pp. 5816–5821.

[16] C. Yoon, H. Bai, X. Wang, C. L. Bak, and F. Blaabjerg, "Regional modeling approach for analyzing harmonic stability in radial power electronics based power system," in *Power Electronics for Distributed Generation Systems (PEDG)*. IEEE, 2015, pp. 1–5.

[17] W. Cao, Y. Ma, and F. Wang, "Sequence-impedance-based harmonic stability analysis and controller parameter design of three-phase inverter-based multibus AC power systems," *IEEE Trans. Power Electron.*, vol. 32, no. 10, pp. 7674–7693, Oct. 2017.

[18] J. Sun, "Impedance-based stability criterion for grid-connected inverters," *IEEE Trans. Power Electron.*, vol. 26, no. 11, pp. 3075–3078, Nov. 2011.

[19] H. Liu, X. Xie, and W. Liu, "An oscillatory stability criterion based on the unified *dq*-frame impedance network model for power systems with high-penetration renewables," *IEEE Trans. Power Syst.*, vol. 33, no. 3, pp. 3472–3485, May 2018.

[20] H. Liu and X. Xie, "Impedance network modeling and quantitative stability analysis of sub-/super-synchronous oscillations for large-scale wind power systems," *IEEE Access*, vol. 6, pp. 34 431–34 438, 2018.

[21] W. Zhou, Y. Wang, and Z. Chen, "Impedance-based modelling method for length-scalable long transmission cable for stability analysis of grid-connected inverter," in *South Power Electronics Conferences (SPEC)*. IEEE, 2018, Accepted.